Synthesis and Crystallization Behavior of Poly(*m*-methylene 2,6-naphthalate-*co*-1,4-cyclohexylenedimethylene 2,6-naphthalate) Copolymers

Young Gyu Jeong and Won Ho Jo*

Hyperstructured Organic Materials Research Center and School of Materials Science and Engineering, Seoul National University, Seoul 151-742, Korea

Sang Cheol Lee

School of Advanced Materials and Systems Engineering, Kumoh National University of Technology, Kumi 730-701, Korea

Received January 24, 2003; Revised Manuscript Received April 8, 2003

ABSTRACT: A series of poly(*m*-methylene 2,6-naphthalate-*co*-1,4-cyclohexylenedimethylene 2,6-naphthalate) copolymers were synthesized, and their crystallization behavior was investigated using differential scanning calorimetry (DSC) and wide-angle X-ray diffraction (WAXD). Poly(ethylene 2,6-naphthalate-*co*-1,4-cyclohexylenedimethylene 2,6-naphthalate) (P(EN-*co*-CN)) copolymers do not crystallize in the middle of copolymer composition, whereas poly(buthylene 2,6-naphthalate-*co*-1,4-cyclohexylenedimethylene 2,6-naphthalate) (P(BN-*co*-CN)) and poly(hexamethylene 2,6-naphthalate-*co*-1,4-cyclohexylenedimethylene 2,6-naphthalate) (P(HN-*co*-CN)) copolymers show clear melting and crystallization peaks in DSC thermograms and sharp diffraction peaks in WAXD patterns for all copolymer compositions, indicating that both P(BN-*co*-CN) and P(HN-*co*-CN) copolymers show cocrystallization behavior. Furthermore, P(BN-*co*-CN) copolymers exhibit an eutectic melting point in the plot of melting temperature vs copolymer composition, and their WAXD patterns are divided into two classes according to the copolymer composition, i.e., PBN-type and PCN-type diffraction patterns. This indicates that P(BN-*co*-CN) shows isodimorphic cocrystallization. On the other hand, the melting temperature of P(HN-*co*-CN) copolymer increases continuously with increasing CN content without showing an eutectic melting temperature, indicating that P(HN-*co*-CN) copolymer shows isomorphic cocrystallization behavior.

Introduction

As the 2,6-naphthalenedicarboxylic acid monomer has been commercially available in large-scale quantity, poly(*m*-methylene 2,6-naphthalate)s (*m* denotes the number of methylene groups) with the chemical structure as shown in Figure 1a have recently attracted much attention from both industry and academia. Among poly(*m*-methylene 2,6-naphthalate)s, two polymers, poly(ethylene 2,6-naphthalate) (PEN, $m = 2$) and poly(butylene 2,6-naphthalte) (PBN, $m = 4$), are intensively studied due to their good thermal, mechanical, gas barrier, and chemical resistant properties. It was found that PEN[1−3] and PBN[4,5] have two different crystal structures depending upon temperature and/or external stress, as listed in Table 1. Recently, we have investigated the crystal structure and thermal properties of poly(hexamethylene 2,6-naphthalate) (PHN, $m = 6$).[6,7] It was observed that melting and glass transition temperatures of PHN are 209 and 45 °C, respectively, and its overall crystallization rate is faster than that of PEN but slightly slower than that of PBN. Therefore, PHN can be used as an engineering thermoplastic. It was also identified that PHN has two crystal structures depending upon the crystallization temperature, as listed in Table 1.

Instead of the methylene group in poly(*m*-methylene 2,6-naphthalate), introduction of the 1,4-cyclohexylenedimethyl group, a thermally stable and rigid unit, is expected to give better thermal and mechanical properties to the resulting polymer, poly(1,4-cyclohexylenedimethylene 2,6-naphthalate) (PCN) (Figure 1b), as compared to PEN, PBN, and PHN. Moreover, 1,4-cyclohexanedimethanol (CHDM), a monomer of PCN, is now commercially produced by industry. This leads us to investigate the structure and properties of PCN. We have identified the crystal structure and thermal transition temperatures of PCN by using wide-angle X-ray diffraction (WAXD) and differential scanning calorimetry (DSC), respectively.[8] The glass transition and melting temperatures of PCN were 110 and 320 °C, respectively. These high transition temperatures would make it difficult to process the polymer in melt. Therefore, it is needed to lower the transition temperatures to some extent.

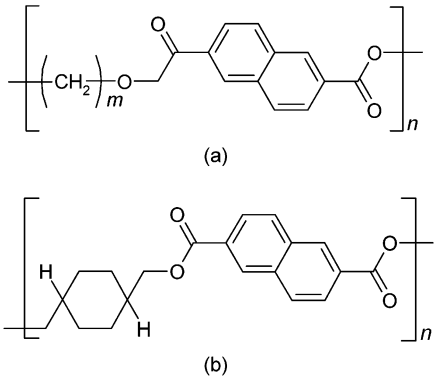

Figure 1. Chemical structures of (a) poly(*m*-methylene 2,6-naphthalate) and (b) poly(1,4-cyclohexylenedimethylene 2,6-naphthalate).

Copolymerization and reactive blending of polyesters have been a convenient method of controlling their thermal and mechanical properties through variation of the composition of copolyesters.[9−15] In most of copoly-

* To whom correspondence should be addressed: Tel 82-2-880-7192; Fax 82-2-885-1748; e-mail whjpoly@plaza.snu.ac.kr.

10.1021/ma034094j CCC: $25.00
Published on Web 05/09/2003

Table 1. Crystallographic Data for PEN, PBN, PHN, and PCN

	PEN[1−3]		PBN[4,5]		PHN[6,7]		
	α-form	*β*-form	A-form	B-form	α-form	*β*-form	PCN[8]
crystal system	triclinic	triclinic	triclinic	triclinic	triclinic	triclinic	triclinic
a (nm)	0.651	0.926	0.487	0.455	0.599	0.670	0.638
b (nm)	0.575	1.559	0.622	0.643	0.589	0.566	0.657
c (nm)	1.320	1.273	1.436	1.531	1.857	1.840	1.661
unit cell parameters							
α (deg)	81.33	121.6	100.78	110.1	73.0	79.0	83.41
β (deg)	144.0	95.57	126.90	121.1	139.0	145.0	43.92
γ (deg)	100.0	122.52	97.93	100.6	91.1	90.0	106.02
repeating unit/unit cell	1	4	1	1	1	1	1
unit cell density (g cm^{-3})	1.407	1.439	1.386	1.395	1.273	1.313	1.313
unit cell volume (nm^3)	0.286	1.121	0.324	0.322	0.389	0.377	0.410

mers where both A and B components are crystallizable, the degree of crystallinity decreases as the composition of minor component increases, so that the copolymers often become totally amorphous even at low comonomer content due to the incompatibility of two components in crystal lattice. If two crystallizable components of copolymer are compatible in each crystal lattice (i.e., cocrystallization), it is expected that thermal and mechanical properties of the copolymer can be controlled without significant loss of crystalline properties through variation of the copolymer composition.

Cocrystallization behavior in A−B random copolymers consisting of two crystallizable components is largely classified into two types, i.e., isomorphism and isodimorphism. When two components of A and B have the similar chemical structure and thus occupy approximately the same volume, the excess free energy of cocrystallization would be very small, and therefore the chain conformation of both corresponding homopolymers becomes compatible with either crystal lattice. As a result, only one crystalline phase containing both comonomer units is observed over all copolymer compositions, and therefore a minimum eutectic melting temperature may not exist in the plot of melting temperature vs copolymer composition. This behavior is referred to as isomorphism.[16] On the other hand, copolymers may show isodimorphism where two crystalline phases are observed. This isodimorphism is subdivided into two cases. One is the case where each of crystalline phases contains comonomer units: incorporation of B components in A crystal lattice, and vice versa. The other case is that the A component can cocrystallize with incorporation of the B component, whereas the B component crystallizes with complete rejection of the A component. In both cases of isodimorphism, the increase of minor comonomer concentration in each crystalline phase is accompanied by lowering of the melting temperature and the crystallinity of copolymer. As a result, a minimum eutectic melting temperature is observed in the plot of melting temperature vs copolymer composition. Thermodynamic phase diagrams of isomorphic and isodimorphic cocrystallization for A−B random copolymers are well documented in ref 17.

In this study, a series of poly(*m*-methylene 2,6-naphthalate-*co*-1,4-cyclohexylene dimethylene 2,6-naphthalalate) ($m = 2$, 4, and 6) copolymers were synthesized and characterized using ^{1}H NMR spectroscopy and viscometry, and their crystallization behavior was systematically investigated by using DSC and WAXD.

Experimental Section

Synthesis and Characterization of Materials. A series of P(EN-*co*-CN), P(BN-*co*-CN), and P(HN-*co*-CN) copolymers with various copolymer compositions were synthesized from ethylene glycol (EG), 1,4-butanediol (BD), 1,6-hexanediol (HD), 1,4-cyclohexanedimethanol (CHDM), and dimethyl 2,6-naphthalate (DMN) using titanium isopropoxide as a catalyst. Commercially available CHDM monomer, a mixture of trans/cis (70/30) isomers, is used without further purification in this study. Two-step reaction was performed on a laboratory-scale polymerization reactor. The first-step reaction was the transesterification at 170−280 °C under a nitrogen atmosphere, and the degree of transesterification was monitored by the amount of distilled methanol as a byproduct. The second step was the polycondensation reaction at 280−350 °C under high-vacuum conditions. At the end of reaction, the product in the melt was quenched into cold water and then dried in a vacuum oven for several days.

The intrinsic viscosities of all the samples were measured in a mixed solvent of phenol and 1,1,2,2-tetrachloroethane (6/4, v/v) using an Ubbelohde viscometer at 35 °C. ^{1}H NMR spectroscopy was used for determining both the copolymer composition and the degree of randomness of the copolymers. ^{1}H NMR spectra of the samples in $CDCl_3$/CF_3COOD (5/5, v/v) solutions were obtained using on a Bruker AMX500 FT-NMR spectrometer operating at 500 MHz and using tetramethylsilane (TMS) as the internal standard.

Thermal Analysis. The crystallization and melting behavior of the samples was measured using a Perkin-Elmer DSC-7 equipped with an intercooler. Temperature and heat flow were calibrated using high-purity indium standard (156.6 °C and 28.45 J/g). The melt-quenched sample was prepared by heating to the temperature 30 °C higher than its melting temperature, holding for 3 min, and then quenching into liquid nitrogen. A small sample size of 5 ± 0.2 mg was used to minimize the effect of thermal conductivity of polymer. Heating and cooling rates were 20 °C/min and 10 °C/min, respectively. The peak temperature of melting and crystallization of the sample was taken as the apparent melting and crystallization temperature, respectively.

To determine the equilibrium melting temperature ($T_m°$) of the sample, isothermal crystallization was carried out on DSC at various crystallization temperatures (T_c). The sample was heated to the temperature 30 °C higher than its respective apparent melting temperature, held for 3 min in order to completely melt the crystal, and rapidly cooled to the predetermined crystallization temperature (T_c) at a rate of 200 °C/min. The melting temperature (T_m) of isothermally crystallized sample was determined from the following heating thermogram. The $T_m°$'s for all the samples were determined from the Hoffman−Weeks plot.[18]

WAXD Analysis. The X-ray diffractograms were obtained using a MAC Science M18XHF diffractometer with Ni-filtered Cu Kα radiation ($\lambda = 0.154$ nm, 50 kV, 100 mA) at scanning rate of 2°/min. The diffractometer was equipped with a $\theta/2\theta$ goniometer, a divergence slit (1.0°), a scattering slit (1.0°), and a receiving slit (0.30 mm). The angular calibration was performed with Si powder ($2\theta = 28.44°$) as a standard. The sample for obtaining the X-ray diffractogram was prepared in film. All samples were compression-molded into 0.4 mm thick film on a hot press at a temperature 30 °C higher than the apparent melting temperature of the respective sample, rapidly transferred on the other hot press at a temperature

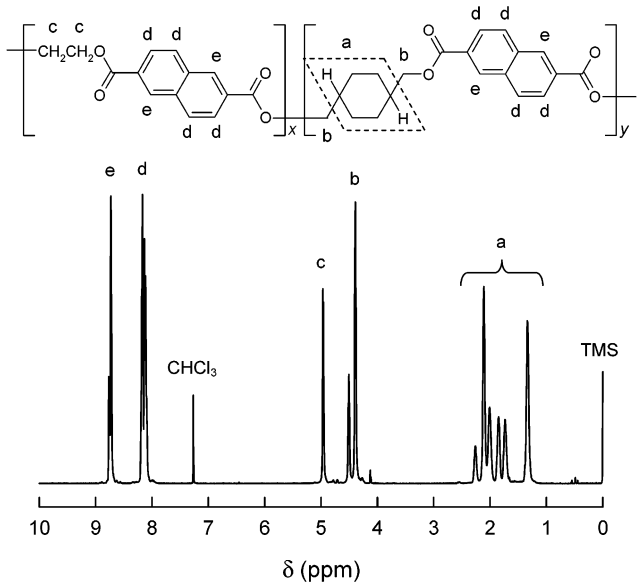

Figure 2. A typical ^{1}H NMR spectrum of P(EN-*co*-CN) copolymer with its peak assignment.

Table 2. Composition and Intrinsic Viscosities of P(EN-*co*-CN) Copolymers

sample code	feed composition (mol %) EN	feed composition (mol %) CN	copolymer composition[a] (mol %) EN	copolymer composition[a] (mol %) CN	intrinsic viscosity (dL/g)
PEN	100.0	0.0	100.0	0.0	0.74
P(EN-*co*-16 CN)	90.0	10.0	84.4	15.6	0.73
P(EN-*co*-23 CN)	80.0	20.0	77.4	22.6	0.71
P(EN-*co*-35 CN)	70.0	30.0	64.6	35.4	0.72
P(EN-*co*-52 CN)	50.0	50.0	37.7	52.3	0.57
P(EN-*co*-71 CN)	35.0	65.0	28.8	71.2	0.48
P(EN-*co*-94 CN)	15.0	85.0	6.2	93.8	0.43
PCN	0.0	100.0	0.0	100.0	0.48

[a] Measured by ^{1}H NMR.

20 °C lower than their respective melting temperature, and then isothermally crystallized for several hours.

Results and Discussion

Characterization of Copolymers. A ^{1}H NMR spectrum of P(EN-*co*-CN) copolymer with assignment of each peak is shown in Figure 2. The copolymer composition was calculated by using following equation:

$$\frac{c}{b} = \frac{X}{Y} \quad \text{or} \quad \frac{d}{b} = \frac{2e}{b} = \frac{X+Y}{Y} \tag{1}$$

where *a*, *b*, *c*, *d*, and *e* represent the areas of corresponding peaks in Figure 2, and *X* and *Y* indicate the mole fractions of EN and CN units, respectively. When the copolymer composition calculated by eq 1 is compared with the feed composition, the EN content in the copolymer determined by ^{1}H NMR is smaller than that in the feed, as listed in Table 2. The reason is probably because EG is more volatile than CHDM during the polycondensation reaction, as noted by Sun et al.[14]

A typical ^{1}H NMR spectrum of P(BN-*co*-CN) copolymer with assignment of each peak is shown in Figure 3. When the copolymer composition of P(BN-*co*-CN) is calculated by using eq 1, the BN content in the copolymer is smaller than that in the feed, as listed in Table 3. This is also explained by the fact that BD is more volatile than CHDM during polycondensation reaction. The resonances between 8.6 and 8.8 ppm in NMR

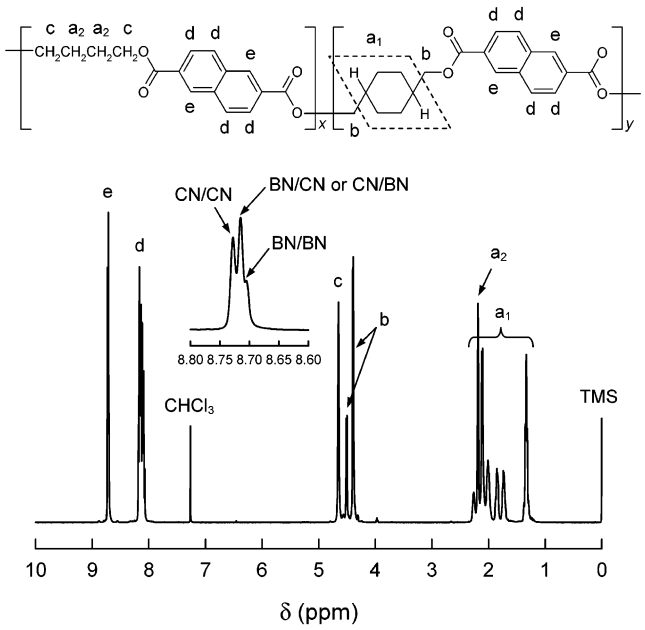

Figure 3. A typical ^{1}H NMR spectrum of P(BN-*co*-CN) copolymer with its peak assignment.

Table 3. Composition and Intrinsic Viscosities of P(BN-*co*-CN) Copolymers

sample code	feed composition (mol %) BN	feed composition (mol %) CN	copolymer composition[a] (mol %) BN	copolymer composition[a] (mol %) CN	intrinsic viscosity (dL/g)	deg of randomness (DR)
PBN	100.0	0.0	100.0	0.0	0.69	
P(BN-*co*-15 CN)	90.0	10.0	85.0	15.0	0.68	1.02
P(BN-*co*-30 CN)	75.0	25.0	71.1	29.9	0.61	1.06
P(BN-*co*-41 CN)	65.0	35.0	59.4	40.6	0.62	0.99
P(BN-*co*-61 CN)	45.0	55.0	39.8	61.2	0.57	1.05
P(BN-*co*-85 CN)	25.0	75.0	14.6	85.4	0.63	1.04
PCN	0.0	100.0	0.0	100.0	0.48	

[a] Measured by ^{1}H NMR.

spectra can be used to determine the number-average sequence length and the degree of randomness (DR) of the P(BN-*co*-CN) copolymer. An expanded ^{1}H NMR spectrum in the range 8.6−8.8 ppm is also shown in the inset of Figure 3, where three peaks are assigned to BN/BN (8.698 ppm), BN/CN (8.714 ppm), and CN/CN (8.726 ppm) dyads. The relative concentrations of the three dyads are determined from the areas of three deconvoluted peaks. From the three peak areas ($A_{BN/BN}$, $A_{BN/CN}$, and $A_{CN/CN}$) corresponding to BN/BN, BN/CN, and CN/CN dyads, the number-average sequence lengths (L_{BN} and L_{CN}) of BN and CN are calculated using the following equations:[19,20]

$$L_{BN} = \frac{2A_{BN/BN} + A_{CN/BN}}{A_{CN/BN}} = \frac{1}{P_{CN/BN}} \tag{2}$$

$$L_{CN} = \frac{2A_{CN/CN} + A_{BN/CN}}{A_{BN/CN}} = \frac{1}{P_{BN/CN}} \tag{3}$$

where $P_{i/j}$ denotes the probability of finding an *i* unit next to a *j* unit in the copolymer chain. The degree of randomness, DR, of the copolymers is defined as[19,20]

$$DR = P_{BN/CN} + P_{CN/BN} = 1/L_{BN} + 1/L_{CN} \tag{4}$$

By definition, DR = 0 is for a homopolymer mixture and virtually for pure block copolymer, and DR = 1 is for a

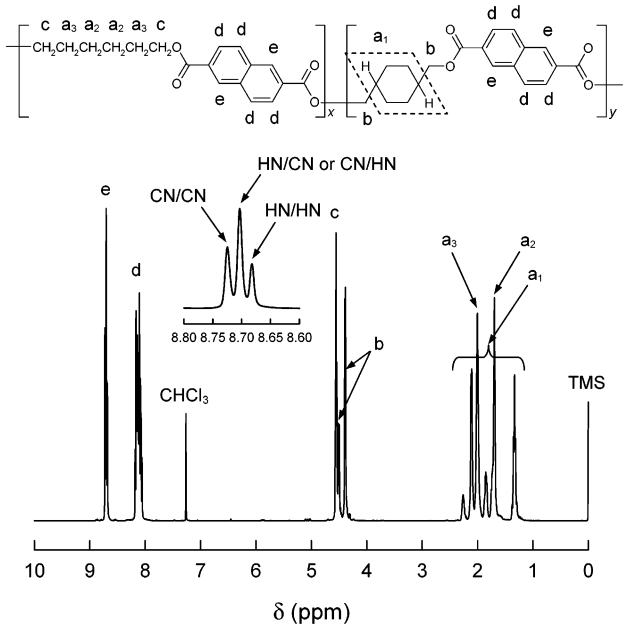

Figure 4. A typical ^{1}H NMR spectrum of P(HN-*co*-CN) copolymer with its peak assignment.

Table 4. Composition and Intrinsic Viscosities of P(HN-*co*-CN) Copolymers

	feed composition (mol %)		copolymer composition[a] (mol %)		intrinsic viscosity	deg of randomness
sample code	HN	CN	HN	CN	(dL/g)	(DR)
PHN	100.0	0.0	100.0	0.0	0.71	
P(HN-*co*-17 CN)	85.0	15.0	83.4	16.6	0.69	1.01
P(HN-*co*-28 CN)	75.0	25.0	71.7	28.3	0.61	1.02
P(HN-*co*-41 CN)	60.0	40.0	58.5	41.5	0.59	1.02
P(HN-*co*-57 CN)	45.0	55.0	42.7	57.3	0.57	1.02
P(HN-*co*-78 CN)	25.0	75.0	22.2	77.8	0.58	1.00
P(HN-*co*-95 CN)	10.0	90.0	5.5	94.5	0.49	0.92
PCN	0.0	100.0	0.0	100.0	0.48	

[a] Measured by ^{1}H NMR.

random copolymer, indicating that the distribution of comonomer units obeys the Bernoullian statistics. An alternating copolymer, e.g., a chain consisting of only BN/CN dyads, gives a DR value of 2. As can be seen in Table 3, the DR values of P(BN-*co*-CN) copolymers are nearly unity, which indicates that P(BN-*co*-CN) copolymers synthesized in this study are statistically random copolymers.

Figure 4 represents a typical ^{1}H NMR spectrum of P(HN-*co*-CN) copolymer with its peak assignment. The copolymer composition of P(HN-*co*-CN) copolymers calculated by eq 1 is nearly the same as the feed composition, as can be seen in Table 4. An expanded ^{1}H NMR spectrum in the range 8.6−8.8 ppm is also represented in the inset of Figure 4, where three peaks are assigned to HN/HN (8.683 ppm), HN/CN (8.704 ppm), and CN/CN (8.725 ppm) dyads. When the DR values of all P(HN-*co*-CN) copolymers are evaluated using eqs 3 and 4, the values are close to unity, which indicates that P(HN-*co*-CN)s are random copolymers.

The intrinsic viscosities of all the copolymers are in the range 0.43−0.74 dL/g, as listed in Tables 2−4, indicating that the samples synthesized in this study have relatively high molecular weight enough to form in film.

Crystallization Behavior of Copolymers. (i) P(EN-*co*-CN) Copolymers. The heating and cooling thermograms of the melt-quenched P(EN-*co*-CN) are shown in Figure 5. Melting (T_m) and cold-crystallization temperatures (T_{cc}) on heating run as well as melt-crystallization peak (T_{mc}) on cooling run are not observed for P(EN-*co*-CN) copolymers with the middle of copolymer composition, indicating that the copolymers become totally amorphous as the composition of minor component increases. The glass transition temperature (T_g) of the copolymer decreases linearly with increasing the CN comonomer content, as shown in Figure 6, which provides another evidence that P(EN-*co*-CN)s are random copolymers. It is noted that the melting temperature of PCN decreases with increasing the EN content up to 30 mol %.

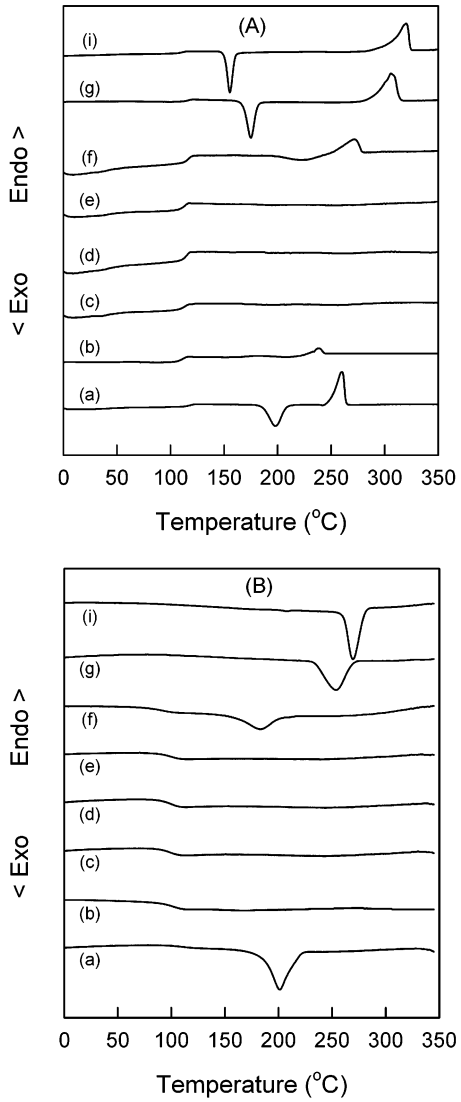

Figure 5. DSC heating (A) and cooling (B) thermograms of melt-quenched samples: (a) PEN; (b) P(EN-*co*-16 CN); (c) P(EN-*co*-23 CN); (d) P(EN-*co*-35 CN); (e) P(EN-*co*-52 CN); (f) P(EN-*co*-71 CN); (g) P(EN-*co*-94 CN); (h) PCN.

WAXD patterns of P(EN-*co*-CN) copolymers, melt-crystallized isothermally under the same degree of undercooling, are shown in Figure 7. The diffraction pattern of PEN in Figure 7 indicates that PEN homopolymer consists of mainly β-form crystals and small fraction of α-form crystal. Similar to the DSC results, there is no significant diffraction peak for the copolymers with the middle of copolymer composition. Therefore, it is concluded from both DSC and WAXD results that the P(EN-*co*-CN) copolymers do not exhibit cocrystallization.

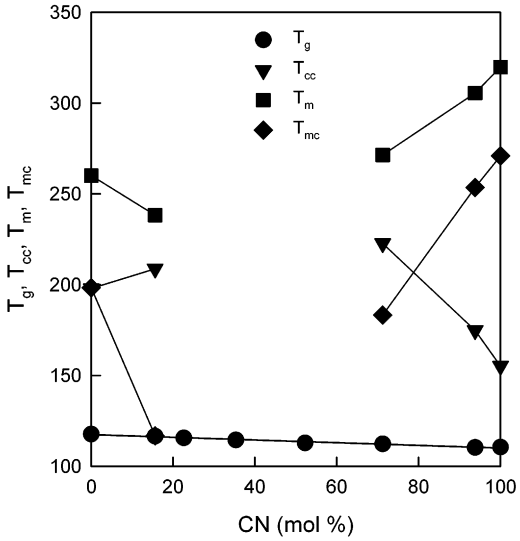

Figure 6. Glass (T_g), cold-crystallization (T_{cc}), melting (T_m), and melt-crystallization temperatures (T_{mc}) of P(EN-*co*-CN) copolymers as a function of copolymer composition.

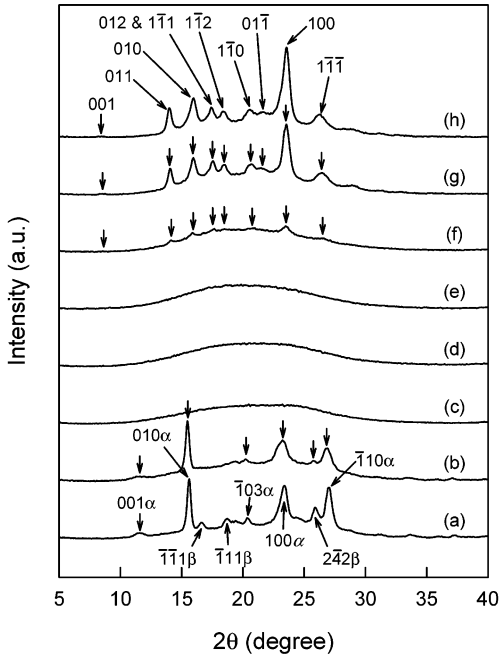

Figure 7. WAXD patterns of the melt-crystallized samples: (a) PEN; (b) P(EN-*co*-16 CN); (c) P(EN-*co*-23 CN); (d) P(EN-*co*-35 CN); (e) P(EN-*co*-52 CN); (f) P(EN-*co*-71 CN); (g) P(EN-*co*-94 CN); (h) PCN.

(ii) P(BN-*co*-CN) Copolymers. Unlike P(EN-*co*-CN), P(BN-*co*-CN) copolymers exhibit clear T_m and T_{cc} on heating run as well as T_{mc} on cooling run over entire copolymer compositions, as shown in Figure 8. This indicates that the copolymers show cocrystallization behavior. Furthermore, the change of the melting and crystallization temperatures with the copolymer composition exhibits a typical eutectic behavior, as shown in Figure 9. This suggests that the P(BN-*co*-CN) copolymers exhibit isodimorphic cocrystallization. Closer examination of Figure 8A reveals that the thermogram of P(BN-*co*-41 CN) shows clear double melting peaks due to melting of both PBN-type and PCN-type crystals, indicating that PBN-type and PCN-type crystals coexist in the copolymer with the composition of 41 mol % CN. This leads us to conjecture that the eutectic composition is around 41 mol %. As can be seen in cooling thermograms of Figure 8B, T_{mc} becomes lower and broader as the composition of minor component in copolymer increases. It means that the crystallization rate of

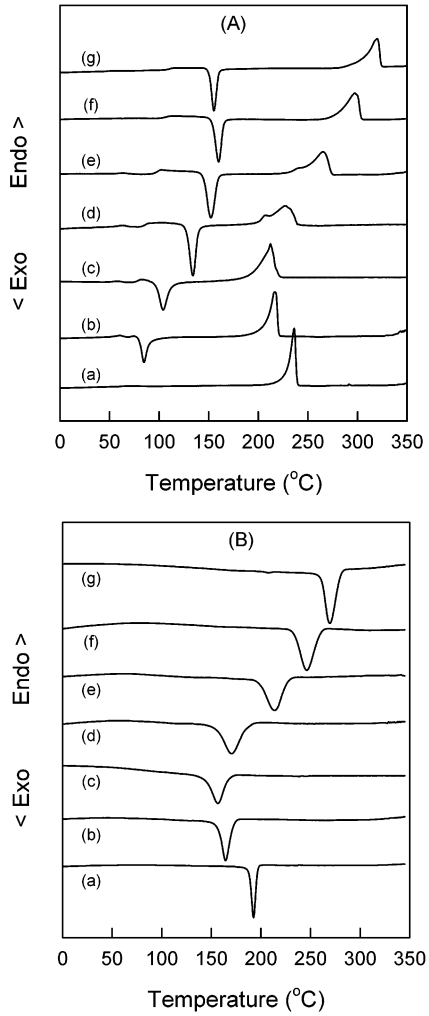

Figure 8. DSC heating (A) and cooling (B) thermograms of melt-quenched samples: (a) PBN; (b) P(BN-*co*-15 CN); (c) P(BN-*co*-30 CN); (d) P(BN-*co*-41 CN); (e) P(BN-*co*-61 CN); (f) P(BN-*co*-85 CN); (g) PCN.

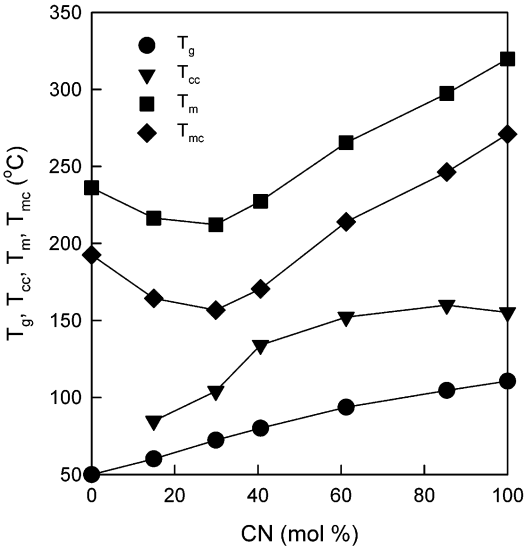

Figure 9. Glass (T_g), cold-crystallization (T_{cc}), melting (T_m), and melt-crystallization temperatures (T_{mc}) of P(BN-*co*-CN) copolymers as a function of copolymer composition.

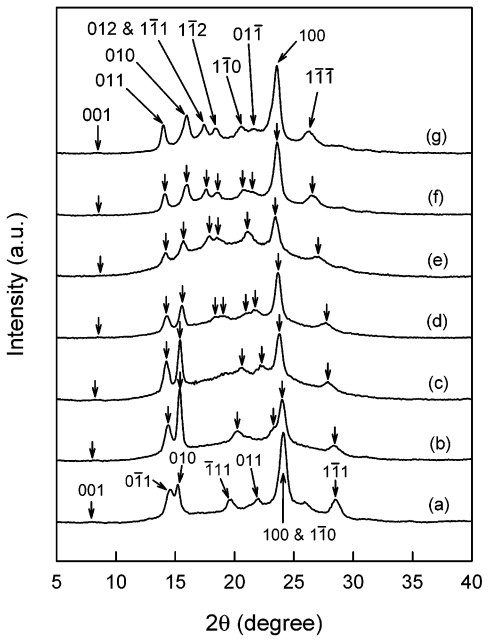

Figure 10. WAXD patterns of melt-crystallized samples: (a) PBN; (b) P(BN-*co*-15 CN); (c) P(BN-*co*-30 CN); (d) P(BN-*co*-41 CN); (e) P(BN-*co*-61 CN); (f) P(BN-*co*-85 CN); (g) PCN.

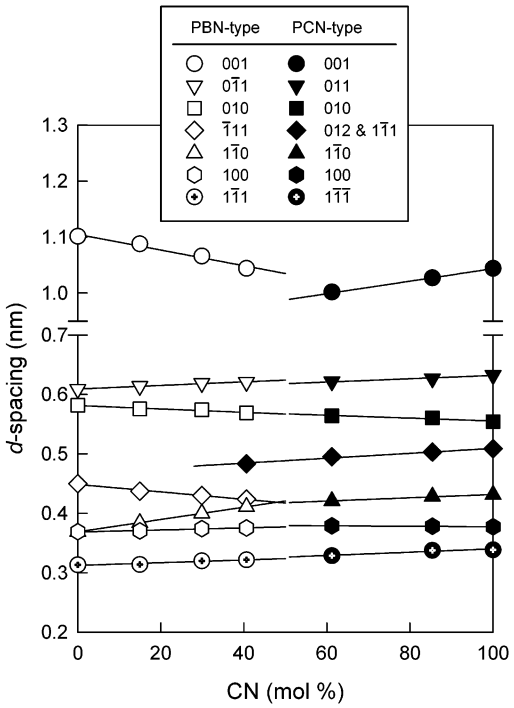

Figure 11. Changes of *d*-spacings for melt-crystallized P(BN-*co*-CN) copolymers with copolymer composition.

copolymer decreases with increasing the content of minor comonomer due to an additional restriction of comonomer on formation of each crystal lattice. When T_gs of P(BN-*co*-CN)s are plotted against the CN comonomer content, T_g increases linearly with increasing of the CN content, as shown in Figure 9. It provides another evidence that P(BN-*co*-CN)s synthesized in this study are random copolymers, as previously evidenced by ^{1}H NMR analysis.

To investigate the change of crystal structure of both PBN and PCN due to cocrystallization with the copolymer composition, the WAXD patterns for the samples melt-crystallized isothermally under the same degree of undercooling are recorded, as shown in Figure 10, where sharp diffraction peaks are observed over the entire range of copolymer composition. The WAXD patterns in Figure 10 can be divided into two classes according to the CN content in the copolymer, i.e., the PBN-type and the PCN-type diffraction patterns. Here, it is noted that the PBN-type crystal is A-form crystal. The PBN-type crystal develops below 41 mol % CN content; i.e., the crystal lattice of PBN accommodates the CN units, and the PCN-type crystal develops above 41 mol % CN content. The WAXD pattern of P(BN-*co*-CN) with 41 mol % CN shows the characteristic diffraction peaks of both PBN and PCN crystals, indicating that the PBN-type and PCN-type crystals coexist in the copolymers with the composition around the eutectic point. Therefore, it is valid to conclude that the crystal transition between PBN-type and PCN-type crystals occurs at the eutectic composition around 41 mol % CN. As a consequence of the corresponding comonomer incorporation in each of PBN-type and PCN-type crystal lattice, *d*-spacings of the crystal lattice change with the corresponding comonomer content, as shown in Figure 11. Particularly, the changes of $d(001)$ and $d(1\bar{1}0)$ of PBN-type and PCN-type crystals with the copolymer composition are discontinuous around the eutectic composition, indicating that P(BN-*co*-CN) exhibits isodimorphic cocrystallization. Also, the change of the two *d*-spacings of PBN-type crystal is much larger than those of PCN-type crystals as the corresponding comonomer content increases. This is probably because the lattice distortion of PBN-type crystal resulting from the incorporation of bulkier CN units in the PBN-type crystal is larger than the opposite case. Note that the volumes of BN and CN units are 0.324 and 0.410 nm^3, respectively, as listed in Table 1. This fact suggests that the unit cell volume of PBN-type crystal increases with increasing the comonomer content whereas the unit cell volume of PCN-type crystal decreases.

Several theories for copolymer crystallization have been developed and can be largely classified into two types: the comonomer exclusion model[21,22] and the comonomer inclusion model.[17,23,24] Wendling and Suter[25] have recently proposed a new model that combines the Sanchez−Eby model[24] (comonomer inclusion model) with the Baur model[22] (comonomer exclusion model). The Wendling−Suter model is given by

$$\frac{1}{T_m(X_B)} - \frac{1}{T_m^\circ} = \frac{R}{\Delta H_m^\circ}\left[\frac{\epsilon X_{CB}}{RT} + (1 - X_{CB})\ln\frac{1 - X_{CB}}{1 - X_B} + X_{CB}\ln\frac{X_{CB}}{X_B} + \langle\tilde{\xi}\rangle^{-1}\right] \quad (5)$$

where T_m° and ΔH_m° denote the equilibrium melting temperature and the heat of fusion of homopolymer, respectively, R the gas constant, X_B the bulk composition of B units in the copolymer, X_{CB} the concentration of comonomer B units in the cocrystal, ϵ the average defect Gibbs free energy, and $\langle\tilde{\xi}\rangle$ the average length of the crystallizable copolymer sequences.

In the equilibrium comonomer inclusion,[23,24] the concentration of comonomer B units in the crystal of A units is given by

$$X_{CB}^{eq} = \frac{X_B e^{-\epsilon/RT}}{1 - X_B + X_B e^{-\epsilon/RT}} \quad (6)$$

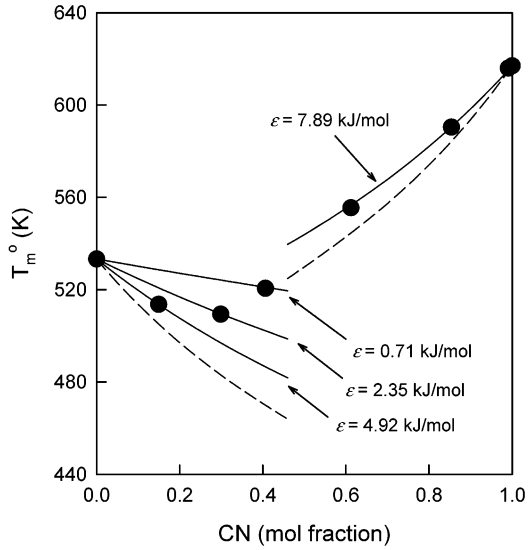

Figure 12. Comparison of the theoretical melting temperatures of P(BN-*co*-CN) copolymers with their equilibrium melting points experimentally determined. Dashed lines and solid lines represent the Baur model and the Wendling−Suter model, respectively.

When X_{eq} in eq 5 is substituted by eq 6, eq 5 is simplified to the following Wendling−Suter equilibrium inclusion model:

$$\frac{1}{T_m^\circ} - \frac{1}{T_m(X_B)} = \frac{R}{\Delta H_m^\circ}[\ln(1 - X_B + X_B e^{-\epsilon/RT}) - \langle\tilde{\xi}\rangle^{-1}] \quad (7)$$

$$\langle\tilde{\xi}\rangle^{-1} = 2(X_B - X_B e^{-\epsilon/RT})(1 - X_B + X_B e^{-\epsilon/RT}) \quad (8)$$

When $X_{CB} = X_B$ and $X_{CB} = 0$ ($\epsilon \rightarrow \infty$), eq 5 is simply changed to the uniform inclusion model and the exclusion model (the Baur model), respectively.

In this study, the Wending−Suter equilibrium inclusion model (eq 5) was employed to determine the defect Gibbs free energy (ϵ) by comparing melting temperatures predicted by the theory with equilibrium melting temperatures (T_m°) of PBN, PCN, and P(BN-*co*-CN)s. It is noted that the ϵ value is used as an adjustable parameter when the melting temperatures predicted by the Wendling−Suter equilibrium inclusion model are compared with experimental ones, as shown in Figure 12. The heat of fusions of PBN and PCN crystals used for fitting work are 33.0 kJ/mol[26] and 34.05 kJ/mol,[27] respectively, and the T_m°'s of PBN and PCN are respectively 533 and 617 K, which are determined by the Hoffman−Weeks plot. When the CN units are incorporated into PBN crystal, the defect Gibbs free energy decreases from 4.92 to 0.71 kJ/mol as the comonomer CN content increases from 15 to 41 mol %, indicating that the comonomer CN unit is easily incorporated into PBN-type crystal lattice as the comonomer CN content increases. This is probably because the CN unit, already incorporated into the PBN crystal lattice, with larger molar volume than that of BN unit creates volume to accommodate the next coming CN unit. On the other hand, when the BN units are incorporated into PCN crystal, the defect free energy is 7.89 kJ/mol. These results lead us to conclude that the defect free energies for incorporation of CN unit into PBN crystal lattice are lower than the opposite case, indicating that that the CN units are more readily incorporated into PBN crystal lattice than the opposite case.

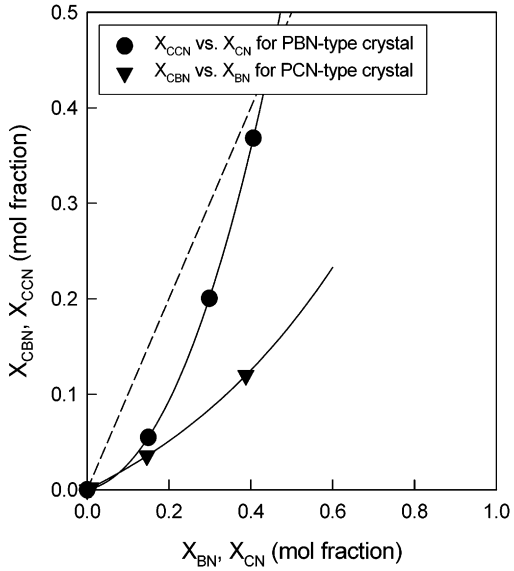

Figure 13. Equilibrium concentrations of CN and BN units incorporated in the respective PBN and PCN crystals as a function of copolymer composition. The dashed line is based on the uniform inclusion model, and the solid lines are based on the polynomial regression.

By using eq 6 with the defect free energies and the T_m°'s of the copolymers determined from the above analysis, the equilibrium concentration (X_{CB}) of comonomer units in the cocrystal can be estimated. When X_{CB} is plotted against X_B, it reveals that the comonomer concentration in each crystal lattice increases with increasing the comonomer composition in bulk, as shown in Figure 13. For both cases, however, the comonomer concentration in each crystal lattice is lower than the comonomer concentration based on the uniform inclusion model ($X_{CB} = X_B$).

(iii) P(HN-*co*-CN) Copolymers. Similar to P(BN-*co*-CN)s, clear T_m and T_{cc} on heating run and T_{mc} on cooling run are observed for all copolymer composition, as shown in Figure 14, indicating that P(HN-*co*-CN)s show cocrystallization behavior. However, unlike P(BN-*co*-CN)s, the eutectic melting point in the plot of melting temperature vs CN comonomer content is not observed, as shown in Figure 15. This indicates that P(HN-*co*-CN)s show isomorphic cocrystallization behavior.

The WAXD patterns for PHN, PCN, and P(HN-*co*-CN)s melt-crystallized isothermally under the same degree of undercooling are shown in Figure 16, where sharp diffraction peaks are observed over the entire range of copolymer composition. When the *d*-spacings of all the reflections are plotted as a function of CN comonomer content, the *d*-spacings change linearly and continuously with the CN comonomer content, as shown in Figure 17. This indicates that the crystal lattice from PHN to PCN changes continuously with variation of copolymer composition. This provides a direct evidence that P(HN-*co*-CN) shows isomorphic cocrystallization behavior.

When the equilibrium melting temperatures of P(HN-*co*-CN)s are plotted as a function of copolymer composition, there exists a minimum point at the copolymer composition of 17 mol % CN, as shown in Figure 18. This minimum point is not the eutectic melting temperature due to the isodimorphic cocrystallization but is due to the polymorphic behavior of PHN. PHN has two different crystal structure, α-form and β-form, depending upon the crystallization conditions, as listed

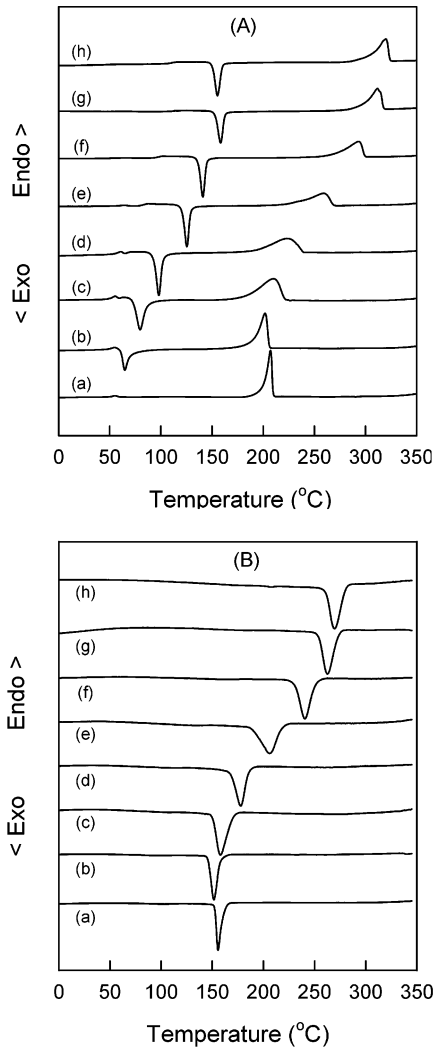

Figure 14. DSC heating (A) and cooling (B) thermograms of melt-quenched samples: (a) PHN; (b) P(HN-*co*-17 CN); (c) P(HN-*co*-28 CN); (d) P(HN-*co*-42 CN); (e) P(HN-*co*-57 CN); (f) P(HN-*co*-78 CN); (g) P(HN-*co*-95 CN); (h) PCN.

in Table 1. Closer examination of WAXD patterns in Figure 16 reveals that the crystal structure of PHN is β-form whereas P(HN-*co*-CN) copolymers show α-form crystal. Here it is expected that the equilibrium melting temperature of PHN β-form crystal is higher than that of PHN α-form crystals because the packing density of β-form crystal is larger than that of α-form crystal.[7,28] Above 17 mol % CN, the equilibrium melting temperature increases with increasing the CN comonomer content. Therefore, it is concluded from DSC and WAXD results that P(HN-*co*-CN) shows isomorphic cocrystallization behavior. Although the chemical structure and conformation of HN unit is quite different from that of CN unit, P(HN-*co*-CN) shows isomorphic cocrystallization. This is probably because the repeating length (*c*-axis), density, and volume of HN unit are quite similar to those of CN unit. Finally, it is noteworthy that P(HN-*co*-CN) is the first reported copolyester showing isomorphic cocrystallization. Indeed, the isomorphic cocrystallization is a very rare phenomenon and has not been reported for polyesters until now.

Conclusions

A series of P(EN-*co*-CN), P(BN-*co*-CN), and P(HN-*co*-CN) copolymers with various CN contents were synthesized, and their crystallization behavior was investigated using DSC and WAXD. P(EN-*co*-CN) copolymers do not crystallize in the middle of copolymer composition, whereas P(BN-*co*-CN) and P(HN-*co*-CN) random copolymers show clear melting and crystallization peaks in DSC thermograms and sharp diffraction peaks in WAXD patterns for all copolymer compositions. These facts indicate that P(BN-*co*-CN)s and P(HN-*co*-CN)s show cocrystallization behavior.

P(BN-*co*-CN)s exhibit an eutectic melting point in the plot of melting temperature vs copolymer composition, indicating that the P(BN-*co*-CN)s show isodimorphic cocrystallization behavior. This isodimorphic cocrystallization behavior is also supported by the fact that WAXD patterns are largely divided into two classes according to the copolymer composition, i.e., the PBN-

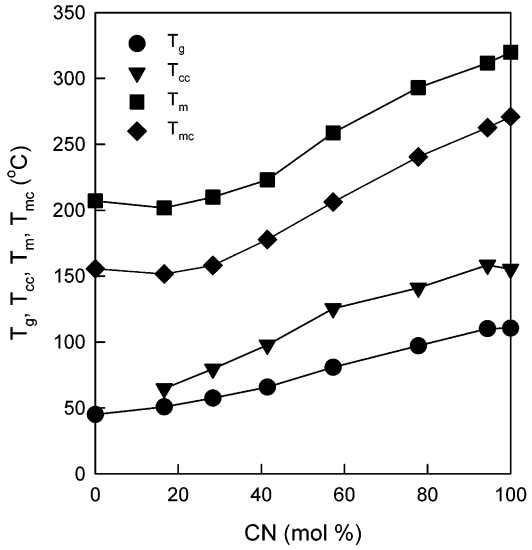

Figure 15. Glass transition (T_g), cold-crystallization (T_{cc}), melting (T_m), and melt-crystallization temperatures (T_{mc}) of P(HN-*co*-CN) copolymers as a function of copolymer composition.

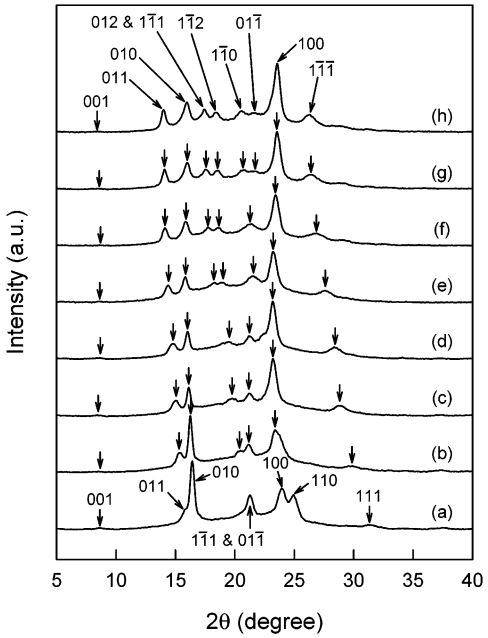

Figure 16. WAXD patterns of melt-crystallized samples: (a) PHN; (b) P(HN-*co*-17 CN); (c) P(HN-*co*-28 CN); (d) P(HN-*co*-42 CN); (e) P(HN-*co*-57 CN); (f) P(HN-*co*-78 CN); (g) P(HN-*co*-95 CN); (h) PCN.

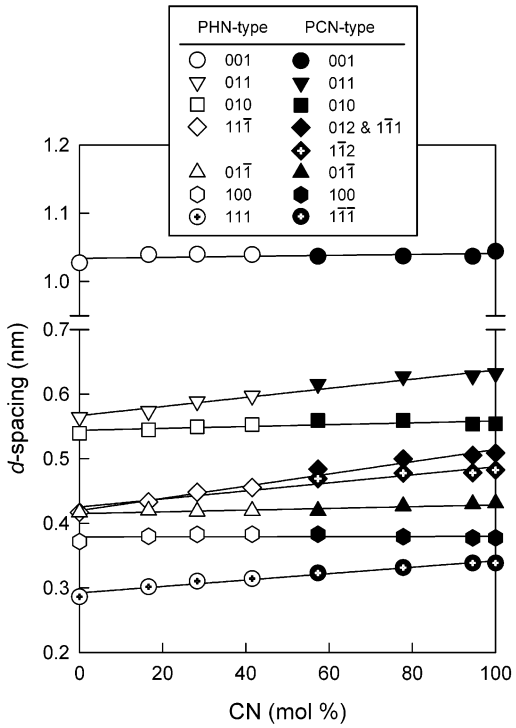

Figure 17. Changes of *d*-spacings for melt-crystallized P(HN-*co*-CN) copolymers with copolymer composition.

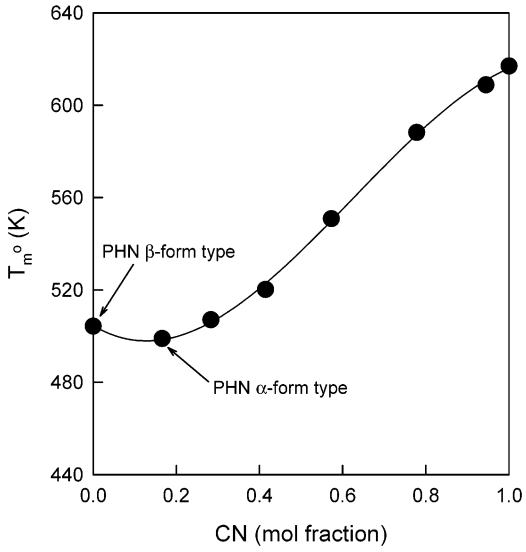

Figure 18. Equilibrium melting temperatures of P(HN-*co*-CN) copolymers. The solid line is based on the polynomial regression.

type and the PCN-type diffraction patterns. The composition at which crystal transition from PBN-type to PCN-type crystal occurs corresponds to the eutectic composition of ca. 41 mol % CN. When the defect Gibbs free energies are estimated by using the equilibrium inclusion model proposed by Wendling and Suter, the defect Gibbs free energy for incorporation of CN unit into the PBN crystal lattice is smaller than the opposite case, indicating that the CN unit is more readily incorporated into the PBN crystal lattice compared to the opposite case.

When the melting temperatures of P(HN-*co*-CN)s are plotted against the copolymer composition, the melting temperature increases continuously with increasing the CN comonomer content without showing an eutectic point. The *d*-spacings of all the diffraction peaks also change linearly with the copolymer composition. These facts lead us to conclude that P(HN-*co*-CN)s show isomorphic cocrystallization behavior. In summary, BN and HN units can cocrystallize with CN unit whereas EN unit cannot. This is because the repeating lengths, volumes, and densities of BN and HN units are comparable to those of CN unit in their respective lattice crystal whereas those of EN unit are not comparable. Since the unit cell density and volume of PHN crystal match better with those of PCN crystal than the density and volume of PBN crystal do, as can be seen in Table 1, P(HN-*co*-CN)s show isomorphic cocrystallization behavior while the P(BN-*co*-CN)s show isodimorphic cocrystallization.

Acknowledgment. The authors thank the Korea Science and Engineering Foundation for financial support through the Hyperstructured Organic Materials Research Center.

References and Notes

(1) Mencik, Z. *Chem. Prum.* **1967**, *17*, 78.
(2) Liu, J.; Myers, J.; Geil, P. H.; Kim, J. C.; Cakmak, M. *SPE Antec. Tech.* **1997**, *43*, 1562.
(3) Buchner, S.; Wiswe, D.; Zachmann, H. G. *Polymer* **1989**, *30*, 480.
(4) Watanabe, H. *Kobunshi Ronbunshu* **1976**, *33*, 299.
(5) Koyano, H.; Yamamoto, Y.; Saito, Y.; Yamanobe, T.; Komoto, T. *Polymer* **1998**, *39*, 4385.
(6) Jeong, Y. G.; Jo, W. H.; Lee, S. C. *Polym. J.* **2001**, *33*, 913.
(7) Jeong, Y. G.; Jo, W. H.; Lee, S. C., unpublished data.
(8) Jeong, Y. G.; Jo, W. H.; Lee, S. C. *Macromolecules*, submitted for publication.
(9) Collins, S.; Kenwright, A. M.; Rawson, C.; Peace, S. K.; Richards, R. W. *Macromolecules* **2000**, *33*, 2974.
(10) Aoki, Y.; Li, L.; Amari, T.; Nishimura, K.; Arashiro, Y. *Macromolecules* **1999**, *32*, 1923.
(11) Papageorgiou, G. Z.; Karayannidis, G. P. *Polymer* **1999**, *40*, 5325.
(12) Montaudo, G.; Puglisi, C.; Samperi, F. *Macromolecules* **1998**, *31*, 650.
(13) Ellis, T. S. *Polymer* **1998**, *39*, 4741.
(14) Sun, Y. M.; Hsu, K. R.; Wang, C. S. *J. Appl. Polym. Sci.* **1998**, *67*, 2245.
(15) Lee, S. C.; Yoon, K. H.; Park, I. H.; Kim, H. C.; Son, T. W. *Polymer* **1997**, *38*, 4831.
(16) Allegra, G.; Bassi, I. W. *Adv. Polym. Sci.* **1969**, *6*, 549.
(17) Kamiya, N.; Sakurai, M.; Inoue, Y.; Chujo, R. *Macromolecules* **1991**, *24*, 3888.
(18) Hoffman, J. D.; Weeks, J. J. *J. Res. Natl. Bur. Stand.* **1962**, *66A*, 13.
(19) Yamadera, R.; Murano, M. *J. Polym. Sci., Polym. Chem. Ed.* **1967**, *5*, 2259.
(20) Koenig, J. L. *Chemical Microstructure of Polymer Chains*; John Wiley and Sons: New York, 1980.
(21) Flory, P. J. *J. Chem. Phys.* **1947**, *15*, 684. (b) Flory, P. J. *Trans. Faraday Soc.* **1955**, *51*, 848.
(22) Baur, V. H. *Makromol. Chem.* **1966**, *98*, 297.
(23) Helfand, E.; Lauritzen, J. I. *Macromoelcules* **1973**, *6*, 631.
(24) Sanchez, I. C.; Eby, R. K. *Macromolecules* **1975**, *8*, 638.
(25) Wendling, J.; Suter, U. W. *Macromolecules* **1998**, *31*, 2516.
(26) Van Krevelen, D. W. *Properties of Polymers*; Elsevier Science Publishers: New York, 1990.
(27) The heat of fusion of PCN with 100% crystallinity was evaluated by measuring the crystallinity (WAXD) and the heat of fusion (DSC) for the samples with different crystallinity.
(28) Jeong, Y. G.; Jo, W. H.; Lee, S. C. *Polymer* **2002**, *43*, 5263.

MA034094J